Vibrational properties and diffusion of hydrogen on graphene

Carlos P. Herrero and Rafael Ramírez
Instituto de Ciencia de Materiales, Consejo Superior de Investigaciones Científicas (CSIC), Campus de Cantoblanco, 28049 Madrid, Spain

(Received 26 November 2008; revised manuscript received 9 February 2009; published 20 March 2009)

Hydrogen and deuterium chemisorption on a single layer of graphene has been studied by path-integral molecular-dynamics simulations. Finite-temperature properties of these point defects were analyzed in the range from 200 to 1500 K by using a tight-binding potential fitted to density-functional calculations. On one hand, vibrational properties of the adatoms are studied at their equilibrium positions linked to C atoms. The vibrations display an appreciable anharmonicity, as derived from the comparison between kinetic and potential energies, as well as between vibrational energy for hydrogen and deuterium. On the other hand, the adatom motion has been studied by quantum transition-state theory. At room temperature, quantum effects are found to enhance the hydrogen diffusivity on the graphene sheet by a factor of 20.

DOI: 10.1103/PhysRevB.79.115429 PACS number(s): 68.43.Pq, 68.43.Jk, 68.43.Fg, 81.05.Uw

I. INTRODUCTION

In recent years, there has been a surge of interest in carbon-based materials. Among them, those formed by C atoms with sp^2 hybridization have been intensively studied, as is the case of carbon nanotubes, fullerenes, and graphene. The latter, in particular, is up to now the only real two-dimensional crystal, with exotic electronic properties.[1,2]

Carbon-based systems, in general, are considered as candidates for hydrogen storage.[3] Also, chemisorption on two-dimensional systems, such as graphene, can be important for catalytic processes.[4] The interest on hydrogen as an impurity in solids and on surfaces is not new and dates back to many years. Even though this is one of the simplest impurities, a thorough understanding of its physical properties is complex due to its low mass and requires the combination of advanced experimental and theoretical methods.[5,6]

Experimental investigations on atomic-isolated hydrogen on graphene have been so far scarce, since H is difficult to detect. Recently, it has been clearly observed by transmission electron microscopy and its dynamics was analyzed in real time.[7] In general, apart from its basic interest as an isolated impurity, an important property of hydrogen in solids and surfaces is its ability to form complexes and passivate defects, which has been extensively studied in the last 20 years.[5,6,8]

From a theoretical viewpoint, atomic hydrogen on graphene has been studied by several authors using *ab initio* methods.[4,9–13] It is generally accepted that the chemisorption of a single hydrogen atom leads to the appearance of a defect-induced magnetic moment on the graphene sheet, along with a large structural distortion.[9–11] However, standard electronic-structure calculations, in spite of their quantum-mechanical character, usually treat atomic nuclei as classical particles, and typical quantum effects as zero-point vibrations are not directly available from the calculations. Such quantum effects may be relevant for vibrational and electronic properties of light impurities such as hydrogen, especially at low temperatures.

Finite-temperature properties of hydrogen-related defects in solids have been studied by *ab initio* and tight-binding (TB) molecular-dynamics simulations. In many earlier applications of these methods, atomic nuclei were treated as classical particles.[14–16] To consider the quantum character of the nuclei, the path-integral molecular-dynamics (PIMD) approach results to be particularly suitable. In this procedure, all nuclear degrees of freedom can be quantized in an efficient way, allowing one to include both quantum and thermal fluctuations in many-body systems at finite temperatures. Thus, the molecular-dynamics sampling applied to evaluate finite-temperature path integrals allows one to carry out quantitative studies of anharmonic effects in condensed matter.[17,18]

In this paper, the PIMD method is used to investigate the role of the impurity mass on the properties of hydrogenic point defects. We study isolated hydrogen and deuterium (D) on a graphene sheet. Special attention has been laid upon the vibrational properties of these impurities by considering anharmonic effects on their quantum dynamics. The results of these calculations show that such anharmonic effects lead to an appreciable deviation of the vibrational energy of the impurities, as compared to a harmonic approximation. Also, the atomic diffusion is found to be enhanced with respect to the classical limit for both H and D. Path-integral methods analogous to that employed in this work have been applied earlier to study hydrogen in metals[17,19,20] and semiconductors.[21–24] In connection with the present work, hydrogen has been studied inside and on carbon nanotubes by diffusion Monte Carlo.[25,26]

The paper is organized as follows. In Sec. II, we describe the computational methods employed in our calculations. Our results are presented in Sec. III, dealing with the energy of the defects, vibrational properties, and impurity diffusion. In Sec. IV we summarize the main results.

II. COMPUTATIONAL METHODS

In this section we present the computational methods employed in our simulations. On one hand, in Sec. II A, we introduce the PIMD method used to obtain equilibrium properties related to the hydrogenic defects. On the other hand, in Sec. II B we discuss a procedure to calculate rate constants

for impurity jumps, in the context of transition-state theory.

A. Path-integral molecular dynamics

Our calculations are based on the path-integral formulation of statistical mechanics, which is a powerful nonperturbative approach to study many-body quantum systems at finite temperatures. In this approach, the partition function is evaluated through a discretization of the density matrix along cyclic paths composed of a number L (Trotter number) of "imaginary-time" steps.[27,28] In the numerical simulations, this discretization gives rise to the appearance of L "beads" for each quantum particle. Then, this method exploits the fact that the partition function of a quantum system can be written in a way formally equivalent to that of a classical one obtained by substituting each quantum particle by a ring polymer consisting of L classical particles connected by harmonic springs.[17,18] Here we employ the molecular-dynamics technique to sample the configuration space of the classical isomorph of our quantum system (N carbon atoms plus one impurity). Calculations were carried out in the canonical ensemble, using an originally developed software, which enables efficient PIMD simulations on parallel computers. The algorithms employed to integrate the equations of motion were based on those described in the literature.[29,30]

The calculations have been performed within the adiabatic (Born-Oppenheimer) approximation, which allows us to define a potential-energy surface for the nuclear coordinates. An important question in the PIMD method is an adequate description of the interatomic interactions, which should be as realistic as possible. Since employing true density functional (DF) or Hartree-Fock-based self-consistent potentials would restrict enormously the size of our simulation cell, we have derived the Born-Oppenheimer surface for the nuclear dynamics from an efficient tight-binding effective Hamiltonian based on DF calculations.[31] The capability of TB methods to reproduce different properties of molecules and solids was reviewed by Goringe *et al.*[32] In particular, the reliability of our TB Hamiltonian to describe hydrogen-carbon interactions in carbon-based materials has been checked in previous work,[24,33] and according to those results we expect that systematic errors in calculated diffusion barriers for H in these materials are less than 0.1 eV. An advantage of the combination of path integrals with electronic-structure methods is that both electrons and atomic nuclei are treated quantum mechanically, so that phonon-phonon and electron-phonon interactions are directly taken into account in the simulation.

Simulations were carried out in the NVT ensemble on a 4×4 graphene supercell of size $4a=9.84$ Å with periodic boundary conditions, containing 32 C atoms and one adatom. For comparison, we also carried out simulations of graphene without impurities, using the same supercell size. We have checked that larger supercells, i.e., 5×5, give within error bars the same results as those derived below from the 4×4 supercell. Sampling of the configuration space has been carried out at temperatures between 200 and 1500 K. For a given temperature, a typical run consisted of 2×10^4 PIMD steps for system equilibration followed by 10^6 steps for the calculation of ensemble-average properties. To have a nearly constant precision in the results at different temperatures, we took a Trotter number that scales as the inverse temperature, so that $LT=6000$ K. For comparison with the results of our PIMD simulations, we have carried out some classical molecular-dynamics simulations with the same interatomic interaction, which is achieved by setting $L=1$. The quantum simulations were performed using a staging transformation for the bead coordinates. Chains of four Nosé-Hoover thermostats were coupled to each degree of freedom to generate the canonical ensemble.[34] The equations of motion were integrated by using the reversible reference system propagator algorithm (RESPA), which allows us to define different time steps for the integration of the fast and slow degrees of freedom.[29] The time step Δt associated to the DF-TB forces was taken in the range between 0.2 and 0.5 fs, which was found to be appropriate for the atomic masses and temperatures studied here. For the evolution of the fast dynamical variables that include the thermostats and harmonic bead interactions, we used a time step $\delta t=\Delta t/4$. More details on the actual implementation of the simulation method can be found elsewhere.[33,35]

B. Quantum transition-state theory

Classical transition-state theory (TST) is a well-established method for calculating rate constants of infrequent events. An important element in this computational method is the ratio between the probability of finding the system at a barrier (saddle point) and at its stable configuration. A quantum extension of this theory has been developed in the context of path integrals, with the purpose of studying the kinetics of processes involving light atoms.[17,36,37] This quantum approach allows one to relate the jump rate k to the probability density of the center of gravity (centroid) of the quantum paths of the jumping atom defined as

$$\bar{\mathbf{x}} = \frac{1}{L}\sum_{i=1}^{L} \mathbf{x}_i, \tag{1}$$

$\mathbf{x}_i$ being the coordinates of the "beads" in the associated ring polymer. Then, k is related to the ratio P_c between the equilibrium probability of finding the centroid at a saddle point (say $\mathbf{x}^*$) and at a stable site (say $\mathbf{x}_0$).[36,38] Namely,

$$k = \frac{\bar{\upsilon} P_c}{2l}, \tag{2}$$

where $\bar{\upsilon}$ is a factor weakly dependent on temperature taken to be the thermal velocity $\bar{\upsilon}=\sqrt{2/(\pi\beta m)}$ of the jumping impurity, and l is the distance between $\mathbf{x}_0$ and $\mathbf{x}^*$. Note that apart of the typical quantum effects, the $1/\sqrt{m}$ factor in $\bar{\upsilon}$ will favor a faster jump rate of the lighter atoms, as in classical TST. The probability ratio P_c can be written as $\exp(-\beta\Delta F)$, ΔF being an effective free-energy barrier, given by the reversible work done on the system when the impurity centroid $\bar{\mathbf{x}}$ moves along a path from $\mathbf{x}_0$ to $\mathbf{x}^*$,

$$\Delta F = -\int_{\mathbf{x}_0}^{\mathbf{x}^*} \mathbf{f}(\bar{\mathbf{x}}) d\bar{\mathbf{x}}, \tag{3}$$

where $\mathbf{f}(\bar{\mathbf{x}})$ is the mean force acting on the impurity with its centroid fixed on $\bar{\mathbf{x}}$ at temperature T,

$$\mathbf{f}(\bar{\mathbf{x}}) = -\langle \nabla_{\mathbf{x}} V(\mathbf{R}) \rangle_{\mathbf{x}}. \tag{4}$$

Here $V(\mathbf{R})$ is the potential energy, $\mathbf{R}$ being in our case a $3(N+1)$-dimensional vector (N carbon atoms plus one impurity). The average value in Eq. (4) is taken over quantum paths with the centroid of the impurity fixed on $\bar{\mathbf{x}}$ at temperature T. Thus, the jump rate (a dynamical quantity) is related to the free-energy difference ΔF (a time-independent quantity), so that its temperature dependence can be obtained from equilibrium simulations without any direct dynamical information.[39] Quantum effects that may give rise to substantial deviations from the classical jump rate are taken into account within this kind of quantum TST. In this way, jump rates for kinetic processes can be obtained for realistic highly nonlinear many-body problems. The reliability of this method to calculate free-energy barriers and jump rates has been discussed in Refs. 19 and 38. In particular, it was argued that this method can be inaccurate in the presence of asymmetric barriers at low temperatures. In our case, the error bar of the calculated barriers is expected to be less than the intrinsic error of the employed tight-binding potential.

In this kind of simulations, the adatom motion was restricted along a reaction coordinate defined by the centroid of the quantum path. Note for comparison that in the equilibrium PIMD simulations described in Sec. II A, there is no restriction on the motion of the H (D) centroid. The force $\mathbf{f}(\bar{\mathbf{x}})$ has been evaluated at 11 points along the reaction coordinate connecting the lowest-energy configuration (H linked to a C atom) with the saddle point of the energy surface and then the integral in Eq. (3) was calculated numerically. For each point in the integration path, we generated 5000 configurations for system equilibration and 2×10^4 configurations for calculating the mean force at a given temperature. More technical details can be found elsewhere.[17,40,41]

III. RESULTS

A. Vibrational energy

We first discuss the lowest-energy configuration for the hydrogenic impurities on a graphene sheet, as derived from classical calculations at $T=0$, i.e., point atomic nuclei without spatial delocalization. The impurity binds to an C atom, which relaxes out of the sheet plane by 0.46 Å, with a bond distance between C and impurity of 1.17 Å. These results are in line with those reported in the literature, and in particular with the breaking of a π bond and producing an additional σ bond, changing the hybridization of the involved C atom from sp^2 to sp^3.[4,10,11] Assuming the host C atoms fixed in the relaxed geometry, one can calculate vibrational frequencies for the impurity in a harmonic approximation. Thus, we find for hydrogen a frequency $\omega_\perp = 2555\ \text{cm}^{-1}$ for stretching of the C-H bond (perpendicular to the graphene sheet) and $\omega_\parallel = 1186\ \text{cm}^{-1}$ for vibrations parallel to the plane (twofold degenerate).

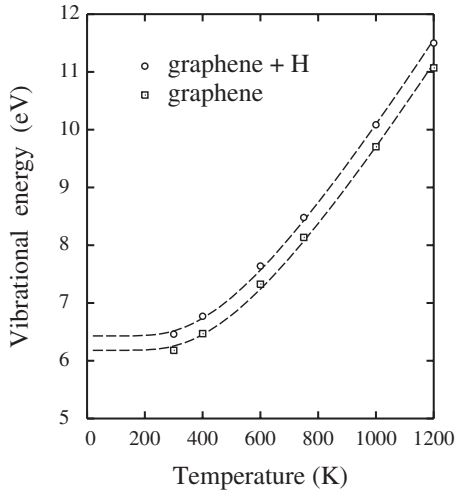

FIG. 1. Temperature dependence of the vibrational energy E_v of the 4×4 graphene supercell with one hydrogen, as derived from PIMD simulations (circles). For comparison, we also present results for a pure graphene supercell (squares). Dashed lines are guides for the eyes. Error bars are in the order of the symbol size.

We now turn to the results of our simulations at finite temperatures and will discuss the energy of the hydrogenic defects. The internal energy of the system graphene plus impurity $E(T)$ at temperature T can be written as

$$E(T) = E_{\text{min}} + E_v(T), \tag{5}$$

where E_{min} is the potential energy for the classical material at $T=0$ (pointlike atoms on their equilibrium positions) and $E_v(T)$ is the vibrational energy of the whole system. Then, $E_v(T)$ can be obtained by subtracting the energy E_{min} from the internal energy derived from PIMD simulations. In Fig. 1 we show the temperature dependence of the vibrational energy E_v for a 4×4 graphene supercell including an H atom (circles). For comparison, we also show E_v for a pure graphene sheet (squares). At 300 K, the vibrational energy of graphene amounts to 6.18 eV per simulation cell, i.e., 0.19 eV/atom. As expected, E_v increases as temperature is raised and eventually converges to the classical limit $E_v^{\text{cl}} = 3Nk_BT$ at high T.

An interesting characteristic of the different hydrogenic defects (H or D) is their associated vibrational energy. At a given temperature, this energy is defined as the difference $\Delta E_v = E_v(32\text{C}+\text{Imp}) - E_v(32\text{C})$, where "Imp" stands for H or D. Note that ΔE_v defined in this way is not just the vibrational energy of a given adatom on graphene but it also includes changes in the vibrations of the nearby C atoms. Shown in Fig. 2 is the vibrational energy associated to the hydrogenic adatoms as a function of temperature. Symbols indicate results of PIMD simulations for H (squares) and D (circles) and dashed lines are guides for the eyes. For comparison, we also present as solid lines the dependence of the vibrational energy of a single particle in a harmonic approximation with the frequencies $\omega_\parallel$ and $\omega_\perp$ given above. At low T, the actual zero-point vibrational energy results to be smaller than that given in the harmonic approach [i.e., $\hbar(\omega_\parallel + \omega_\perp/2)$], but this trend changes as temperature rises. In fact,

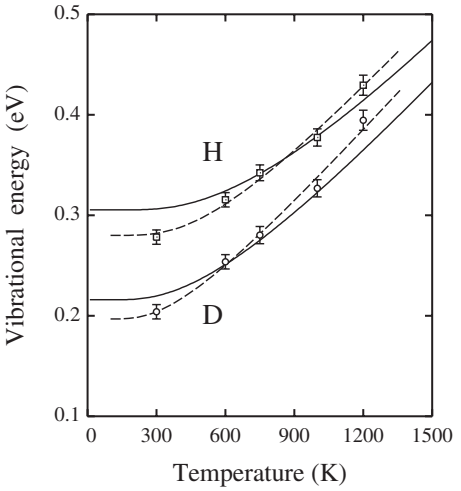

FIG. 2. Vibrational energy ΔE_v of the hydrogenic defects as a function of temperature. Results are shown for hydrogen (squares) and deuterium (circles). For comparison, we also present the vibrational energy obtained in a harmonic approximation with frequencies $\omega_{\parallel}$ and $\omega_{\perp}$ corresponding to H and D (solid lines). Dashed lines are guides for the eyes.

at temperatures larger than 1000 K, the vibrational energy derived from the simulations is larger than that obtained for the one-particle harmonic approach.

Another way of getting insight into the anharmonicity of the defect vibrations is by looking at the ratio $\Delta E_v^{\mathrm{H}}/\Delta E_v^{\mathrm{D}}$ between vibrational energies of point defects for both isotopes. At low temperature, this ratio should converge to $\sqrt{2}$ in the harmonic approximation, going to unity at high temperatures. The results yielded by our simulations are shown in Fig. 3, along with the one-particle harmonic expectancy. The former lies somewhat lower than the latter in the whole temperature region under consideration. In particular, at 300 K we find $\Delta E_v^{\mathrm{H}}/\Delta E_v^{\mathrm{D}}=1.364$ vs a ratio of 1.394 derived in a harmonic approximation.

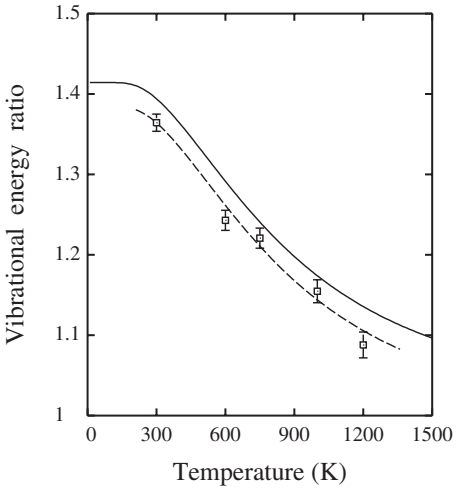

FIG. 3. Temperature dependence of the ratio $\Delta E_v^{\mathrm{H}}/\Delta E_v^{\mathrm{D}}$ between vibrational energies of hydrogen and deuterium defects. Symbols indicate results of PIMD simulations. For comparison, we also present the ratio expected in a one-particle harmonic approximation (continuous line). The dashed line is a guide for the eyes.

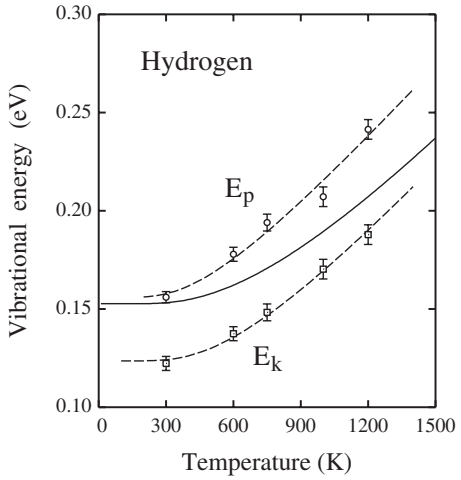

FIG. 4. Temperature dependence of kinetic (squares) and potential (circles) contributions to the vibrational energy of the H defect. A solid line represents the expectancy of a harmonic approximation with frequencies $\omega_{\parallel}$ and $\omega_{\perp}$. Dashed lines are guides for the eyes.

PIMD simulations allow us to separate the potential (E_p) and kinetic (E_k) contributions to the vibrational energy.[42–44] In fact, E_k is related to the spatial delocalization of the quantum paths, which can be obtained directly from the simulations (see below). In Fig. 4, we present the kinetic and potential energies of the point defect associated to hydrogen, as a function of temperature. Symbols indicate results of our simulations for E_k (squares) and E_p (circles), whereas dashed lines are guides for the eyes. The potential energy of the point defect is found to be clearly larger than the kinetic energy, indicating an appreciable anharmonicity of the whole defect (in a harmonic approach, one has $E_k=E_p$). A solid line represents the expected dependence for both kinetic and potential contributions, in a harmonic approximation with the frequencies $\omega_{\parallel}$ and $\omega_{\perp}$ given above. At low temperature, we find an appreciable change in the kinetic energy with respect to the harmonic approach, contrary to the potential energy, which coincides within error bars with the harmonic expectancy. A qualitative understanding of this behavior can be obtained by analyzing the energy changes obtained through time-independent perturbation methods.[22,45] Thus, assuming a perturbed one-dimensional harmonic oscillator (with perturbations of x^3 and x^4 type) at $T=0$, the first-order change in the energy is totally due to a change in the kinetic energy; the potential energy remaining unaltered with respect to its unperturbed value. A similar behavior has been obtained for hydrogen in silicon from path-integral Monte Carlo simulations.[22] The main difference is that in that case the kinetic energy was found to increase with respect to the harmonic value, contrary to the result obtained here for H on graphene. This seems to depend on the details of the interatomic interactions and the actual geometry of the point defect under consideration, but in both cases the potential energy at low temperature is very close to the value yielded by the harmonic approximation.

Path-integral simulations at finite temperatures describe the quantum delocalization through paths of finite size. This means that the average extension of the paths is a measure of

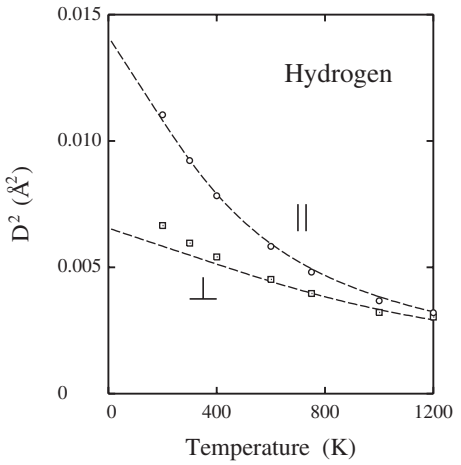

FIG. 5. Mean-square displacement D^2 of the quantum paths for hydrogen in directions parallel (circles) and perpendicular (squares) to the graphene sheet. Dashed lines correspond to a harmonic approximation for vibrations with frequencies $\omega_{\parallel}$ and $\omega_{\perp}$. Error bars of the simulations results are on the order of the symbol size.

the importance of quantum effects in a given problem. One can define a kind of quantum delocalization as the mean-square "radius of gyration" D^2 of the ring polymers associated to the quantum particle under consideration.[17,44] This means

$$D^2 = \frac{1}{L}\left\langle \sum_{i=1}^{L} (\mathbf{x}_i - \bar{\mathbf{x}})^2 \right\rangle, \tag{6}$$

where $\bar{\mathbf{x}}$ is the position of the centroid of the paths defined in Eq. (1), and $\langle \ldots \rangle$ indicates a thermal average at temperature T. Note that the total spatial delocalization of a particle includes an additional term, taking into account displacements of the center of gravity of the paths. This term is the only one surviving at high temperatures, since in the classical limit each path collapses onto a single point. For our problem of hydrogen on graphene, with well-defined H vibrations along three orthogonal axes, one can define a quantum delocalization of hydrogen along each of these directions ($D^2_{\parallel}$ and $D^2_{\perp}$). These delocalizations are displayed in Fig. 5 for vibrations parallel (circles) and perpendicular (squares) to the graphene plane, as derived from our PIMD simulations. D^2 decreases as the temperature is raised and the particle becomes more "classical." For comparison, we also show in Fig. 5 the mean-square displacement D^2 expected for harmonic oscillators of frequencies $\omega_{\parallel}$ and $\omega_{\perp}$, which can be worked out analytically.[17,44,46] The delocalization $D^2_{\parallel}$ derived from the simulations follows closely the harmonic expectancy in the whole temperature range considered here. However, $D^2_{\perp}$ is higher than its corresponding harmonic result at $T<400$ K.

B. Hydrogen diffusion

Hydrogen is expected to diffuse on the graphene sheet, breaking a C-H bond and forming a new one with a nearby C atom. To check the appearance of this kind of hydrogen jumps, we have carried out some classical molecular-dynamics simulations, which allow one to follow the adatom along its trajectory on the surface. As indicated above, this kind of classical limit is easily achieved with our PIMD code by setting the Trotter number $L=1$ (one bead per atom). At temperatures lower than 1000 K, hydrogen jumps on the graphene surface result to be infrequent events and are rarely observed along a simulation run. Then, a reliable estimation of the diffusion coefficient by this method is not possible. Moreover, at temperatures larger than 1000 K hydrogen begins to escape from the sheet, without remaining on it with enough time for studying quantitatively the diffusion process. This situation is remedied by analyzing the hydrogen motion by TST and, in particular, by the quantum version presented in Sec. II B. This procedure allows us to obtain free-energy barriers for impurity jumping, which include corrections due to the quantum character of the atomic nuclei, and in particular the renormalization of the barriers caused by zero-point motion. Also, phonon-assisted tunneling is included in the calculation, since the motion of the C atoms takes into account a full quantization of the vibrational degrees of freedom. The main question we address here is the dependence of hopping rates on temperature and impurity mass. In connection with this, there is a vast literature about theoretical models for quantum diffusion of light particles in solids.[17,47–49] Due to the complexity of this problem, such calculations have been typically based on model potentials for the impurity-lattice interactions.

Here, the jump rate of the impurity between two nearest equilibrium sites is derived from the free-energy barrier between those sites. To calculate this barrier, we first select a continuous path from one site to the other, minimizing the energy at the transition (saddle) point in a classical calculation (pointlike atoms) at $T=0$. In connection with this, it is worthwhile noting that seemingly simple atomic jumps can actually involve coupled barriers, as indicated in Ref. 50. Thus, to obtain the barrier for hydrogen jumps, we considered a coupled motion of H and the nearest C atom. For the optimal path, we obtained an energy barrier of 0.78 eV, with the saddle point corresponding to a symmetric (bridge) configuration of hydrogen between two C atoms and at a distance of 1.7 Å from the graphene plane. Once selected—the best path—we performed finite-temperature path-integral simulations with the centroid of H fixed on several points along this path, as described in Sec. II B. Then, the free-energy barrier is calculated from the mean force by using Eq. (3).

In Fig. 6 we present the free-energy barrier ΔF for adatom diffusion between adjacent C-H bonds. Data derived from line integration of the mean force are shown as a function of temperature for hydrogen (squares) and deuterium (circles). For comparison, we also show results derived from classical simulations (triangles). In this plot, one notices first that ΔF is higher for D than for H and even higher for the classical limit, which in this respect may be considered as the large-mass limit $M \to \infty$.[33,35] Then, we observe an appreciable decrease in the free-energy barrier as the impurity mass is reduced. Second, one observes an increase in ΔF as temperature is raised in the three cases shown in Fig. 6. This increase is smaller but not negligible, in the classical limit, which at $T \to 0$ converges to the potential-energy barrier given above ($\Delta E_p = 0.78$ eV). At low temperature, the de-

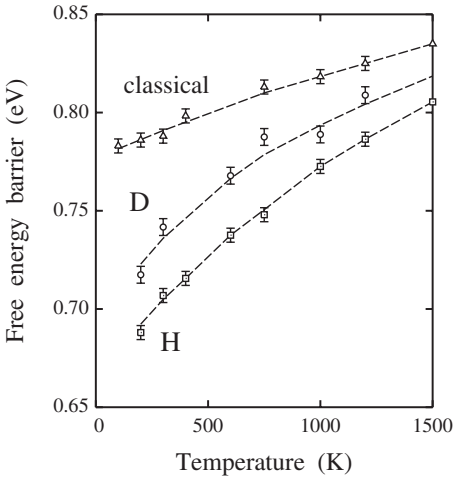

FIG. 6. Effective free-energy barrier for impurity jumps on the graphene sheet as a function of temperature. Squares: hydrogen; circles: deuterium; and triangles: classical limit. Dashed lines are guides for the eyes.

pendence of ΔF upon impurity mass is related to the change in internal energy E of the defect complex along the diffusion path, since then the entropy contribution to the free energy becomes negligible. At 300 K, we find $\Delta F=0.79$, 0.74, and 0.71 eV for the classical limit D and H, respectively. This means that quantum effects renormalize the free-energy barrier at room temperature by about 6% for D and 10% for H. This reduction in ΔF decreases as temperature rises and the atoms become "more classical." In fact, these free-energy barriers should converge one to the other in the high-temperature limit, which cannot be approached here due to the onset of adatom desorption.

Shown in Fig. 7 is the rate for impurity jumps on a graphene sheet as a function of the inverse temperature. Data were derived from the free-energy barriers displayed in Fig. 6 by using Eq. (2). Results are given for hydrogen (squares),

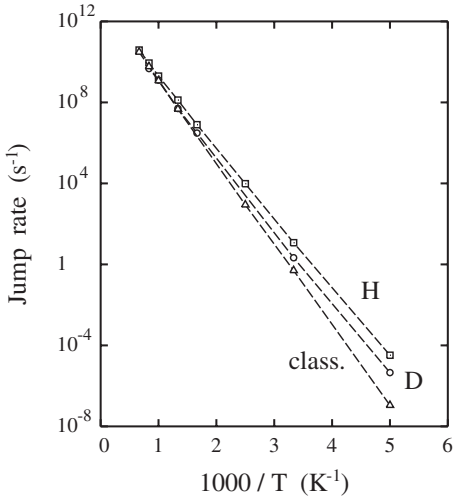

FIG. 7. Rate for impurity jumps on the graphene sheet as a function of the inverse temperature. Symbols represent results derived from simulations for hydrogen (squares), deuterium (circles), and classical limit (triangles). Dashed lines are guides for the eyes.

deuterium (circles), and classical limit (triangles). At $T \leq 500$ K, the jump rate for hydrogen results to be larger than that for deuterium, which in turn is higher than that found in the classical limit, as expected from the change in effective free-energy barrier discussed above. At 300 K, the jump rate for hydrogen is found to be 11.6 s^{-1}, about 20 times larger than the value found in the classical calculation. The influence of quantum effects on hydrogen diffusivity increases as temperature is lowered, as could be expected; but the jump rate itself becomes very small. In fact, at 200 K, the calculated rate for hydrogen k_H is less than 10^{-4} s^{-1}. On the contrary, at high temperatures k_H converges to the classical result, and the difference between both becomes unobservable at T larger than 1000 K. At this temperature, we find $k_H = 2.0 \times 10^9$ s^{-1}.

The diffusion barriers obtained here for H and D on graphene are comparable to those found for hydrogen diffusion on graphite. Ferro *et al.*[51] used density-functional theory to study various diffusion barriers in graphite. For hydrogen diffusion on its surface, they obtained a (classical) barrier of 0.94 eV, somewhat larger than that found here at $T=0$ in the classical limit.

The diffusion of H and D on solid surfaces has been studied earlier using quantum TST, employing simulations similar to those presented here. Such studies were mainly focused on hydrogen diffusion on metal surfaces.[20,52] Our results are qualitatively similar to those obtained in these studies, with an appreciable enhancement of the jump rate of the impurity in comparison to a classical model. At temperatures lower than those studied here ($T<50$ K), a temperature-independent diffusion was found on metal surfaces.[20,53] This is also a possibility for hydrogen diffusion on graphene and remains a challenge for future research. PIMD simulations at those temperatures would need the use of Trotter numbers L larger than 100 that together with the interaction potentials employed here requires computational resources out of the scope of the present work.

IV. SUMMARY

The main advantage of PIMD simulations of hydrogen on graphene is the possibility of calculating defect energies at finite temperatures, including a full quantization of host-atom motions, which are not easy to take into account from fixed-lattice calculations and classical simulations. Isotope effects can be readily explored, since the impurity mass appears as an input parameter in the calculations. This includes the consideration of zero-point motion, which together with anharmonicity may cause appreciable nontrivial effects. Our results indicate that the hydrogen adsorbed on graphene cannot be accurately described as a particle moving in a harmonic potential. Even if anharmonicities of the interatomic potential are taken into account, a single-particle approximation is questionable as a realistic description of impurity complexes at finite temperatures. It is then necessary to treat the defect as a many-body problem with anharmonic interactions.

Ab initio theoretical techniques to calculate defect energies in solids have achieved an excellent precision in recent

years. However, zero-point motion is a factor limiting the accuracy of state-of-the-art techniques to predict energy bands and total energies of solids.[35] The same happens for defect levels caused by impurities in solids, since their energy may change appreciably as the impurity mass is varied. Here, we have illustrated how anharmonicities in the atomic motion cause an appreciable difference between kinetic and potential energies of the defect (about 20% for H at 300 K) and have quantified the effect of the impurity mass on anharmonic shifts in the energy.

Due to the large relaxation of the nearest C atoms, hydrogen migration requires important motion of these atoms. Then, an adatom jump has to be viewed as a cooperative process involving a coupled motion of the impurity and the nearest host atoms. This picture is similar to that described in the literature as an "opening of a door,"[54] which favors impurity diffusion. Thus, the quantum motion of both adatom and C atoms helps to renormalize the diffusion barriers with respect to the classical expectancy. At 300 K, we find a hydrogen diffusivity 20 times larger than that derived from classical barriers.

ACKNOWLEDGMENT

This work was supported by the Ministerio de Ciencia e Innovación (Spain) through Grant No. BFM2003-03372-C03-03.

[1] A. K. Geim and K. S. Novoselov, Nature Mater. **6**, 183 (2007).
[2] M. I. Katsnelson, Mater. Today **10**, 20 (2007).
[3] A. C. Dillon and M. J. Heben, Appl. Phys. A **72**, 133 (2001).
[4] M. H. F. Sluiter and Y. Kawazoe, Phys. Rev. B **68**, 085410 (2003).
[5] S. J. Pearton, J. W. Corbett, and M. Stavola, *Hydrogen in Crystalline Semiconductors* (Springer, Berlin, 1992).
[6] S. K. Estreicher, Mater. Sci. Eng., R. **14**, 319 (1995).
[7] J. C. Meyer, C. O. Girit, M. F. Crommie, and A. Zettl, Nature (London) **454**, 319 (2008).
[8] R. Zeisel, C. E. Nebel, and M. Stutzmann, Appl. Phys. Lett. **74**, 1875 (1999).
[9] O. V. Yazyev and L. Helm, Phys. Rev. B **75**, 125408 (2007).
[10] S. Casolo, O. M. Lovvik, R. Martinazzo, and G. F. Tantardini, J. Chem. Phys. **130**, 054704 (2009).
[11] D. W. Boukhvalov, M. I. Katsnelson, and A. I. Lichtenstein, Phys. Rev. B **77**, 035427 (2008).
[12] E. J. Duplock, M. Scheffler, and P. J. D. Lindan, Phys. Rev. Lett. **92**, 225502 (2004).
[13] P. L. de Andres and J. A. Vergés, Appl. Phys. Lett. **93**, 171915 (2008).
[14] F. Buda, G. L. Chiarotti, R. Car, and M. Parrinello, Phys. Rev. B **44**, 5908 (1991).
[15] G. Panzarini and L. Colombo, Phys. Rev. Lett. **73**, 1636 (1994).
[16] S. Bédard and L. J. Lewis, Phys. Rev. B **61**, 9895 (2000).
[17] M. J. Gillan, Philos. Mag. A **58**, 257 (1988).
[18] D. M. Ceperley, Rev. Mod. Phys. **67**, 279 (1995).
[19] D. E. Makarov and M. Topaler, Phys. Rev. E **52**, 178 (1995).
[20] T. R. Mattsson and G. Wahnström, Phys. Rev. B **51**, 1885 (1995).
[21] R. Ramírez and C. P. Herrero, Phys. Rev. Lett. **73**, 126 (1994).
[22] C. P. Herrero and R. Ramírez, Phys. Rev. B **51**, 16761 (1995).
[23] T. Miyake, T. Ogitsu, and S. Tsuneyuki, Phys. Rev. Lett. **81**, 1873 (1998).
[24] C. P. Herrero and R. Ramírez, Phys. Rev. Lett. **99**, 205504 (2007).
[25] M. C. Gordillo, J. Boronat, and J. Casulleras, Phys. Rev. B **65**, 014503 (2001).
[26] M. C. Gordillo, Phys. Rev. B **76**, 115402 (2007).
[27] R. P. Feynman, *Statistical Mechanics* (Addison-Wesley, New York, 1972).
[28] H. Kleinert, *Path Integrals in Quantum Mechanics, Statistics, and Polymer Physics* (World Scientific, Singapore, 1990).
[29] G. J. Martyna, M. E. Tuckerman, D. J. Tobias, and M. L. Klein, Mol. Phys. **87**, 1117 (1996).
[30] M. E. Tuckerman, in *Quantum Simulations of Complex Many–Body Systems: From Theory to Algorithms*, edited by J. Grotendorst, D. Marx, and A. Muramatsu (NIC, FZ Jülich, 2002), p. 269.
[31] D. Porezag, T. Frauenheim, T. Köhler, G. Seifert, and R. Kaschner, Phys. Rev. B **51**, 12947 (1995).
[32] C. M. Goringe, D. R. Bowler, and E. Hernández, Rep. Prog. Phys. **60**, 1447 (1997).
[33] C. P. Herrero, R. Ramírez, and E. R. Hernández, Phys. Rev. B **73**, 245211 (2006).
[34] M. E. Tuckerman and A. Hughes, in *Classical and Quantum Dynamics in Condensed Phase Simulations*, edited by B. J. Berne and D. F. Coker (Word Scientific, New Jersey, 1998), p. 311.
[35] R. Ramírez, C. P. Herrero, and E. R. Hernández, Phys. Rev. B **73**, 245202 (2006).
[36] G. A. Voth, D. Chandler, and W. H. Miller, J. Chem. Phys. **91**, 7749 (1989).
[37] J. Cao and G. A. Voth, J. Chem. Phys. **100**, 5106 (1994).
[38] M. J. Gillan, J. Phys. C **20**, 3621 (1987).
[39] G. A. Voth, J. Phys. Chem. **97**, 8365 (1993).
[40] C. P. Herrero, Phys. Rev. B **55**, 9235 (1997).
[41] J. C. Noya, C. P. Herrero, and R. Ramírez, Phys. Rev. Lett. **79**, 111 (1997).
[42] M. F. Herman, E. J. Bruskin, and B. J. Berne, J. Chem. Phys. **76**, 5150 (1982).
[43] A. Giansanti and G. Jacucci, J. Chem. Phys. **89**, 7454 (1988).
[44] M. J. Gillan, in *Computer Modelling of Fluids, Polymers, and Solids*, edited by C. R. A. Catlow, S. C. Parker, and M. P. Allen (Kluwer, Dordrecht, 1990), p. 155.
[45] L. D. Landau and E. M. Lifshitz, *Quantum Mechanics*, 2nd ed. (Pergamon, Oxford, 1965).
[46] R. Ramírez and C. P. Herrero, Phys. Rev. B **48**, 14659 (1993).
[47] C. P. Flynn and A. M. Stoneham, Phys. Rev. B **1**, 3966 (1970).
[48] H. Sugimoto and Y. Fukai, Phys. Rev. B **22**, 670 (1980).
[49] H. R. Schober and A. M. Stoneham, Phys. Rev. Lett. **60**, 2307 (1988).

[50] M. Ramamoorthy and S. T. Pantelides, Phys. Rev. Lett. **76**, 267 (1996).
[51] Y. Ferro, F. Martinelli, A. Jelea, and A. Allouche, J. Chem. Phys. **120**, 11882 (2004).
[52] S. W. Rick, D. L. Lynch, and J. D. Doll, J. Chem. Phys. **99**, 8183 (1993).
[53] T. R. Mattsson and G. Wahnström, Phys. Rev. B **56**, 14944 (1997).
[54] D. E. Boucher and G. G. DeLeo, Phys. Rev. B **50**, 5247 (1994).